Dissociation pathways and binding energies of (LiH) n Li+ and (LiH) n Li+ 3 clusters

R. Antoine, Ph. Dugourd, D. Rayane, and M. Broyer

Citation: The Journal of Chemical Physics **104**, 110 (1996); doi: 10.1063/1.470880
View online: http://dx.doi.org/10.1063/1.470880
View Table of Contents: http://scitation.aip.org/content/aip/journal/jcp/104/1?ver=pdfcov
Published by the AIP Publishing

Dissociation pathways and binding energies of $(LiH)_nLi^+$ and $(LiH)_nLi_3^+$ clusters

R. Antoine, Ph. Dugourd, D. Rayane, and M. Broyer
Laboratoire de Spectrométrie Ionique et Moléculaire (URA CNRS n°171), Université Lyon I, Bât 205, 43 Bd du 11 Novembre 1918–69622 Villeurbanne Cedex, France

(Received 11 August 1995; accepted 27 September 1995)

The metastable decomposition of hydrogenated lithium cluster ions $(LiH)_nLi_m^+$ ($m=0$, 1 and 3; $n\leqslant 15$) is studied by using a reflectron mass spectrometer. These clusters are found to decompose by evaporation of a LiH or a Li_2H_2 molecule. The binding energy of these clusters are determined, using a statistical model which has been adapted to mixed clusters. Comparison with other mixed clusters suggests that $(LiH)_nLi^+$ clusters form compact cubic structure similar to pieces of a crystal lattice. For $(LiH)_nLi_3^+$ clusters, the dissociation channels are more surprising, and the localization of the two excess electrons is discussed, as well as the possible existence of an energy barrier for the dissociation. © *1996 American Institute of Physics.* [S0021-9606(96)01401-7]

I. INTRODUCTION

During the last few years, mixed clusters (MX) formed from a metal (M: alkali) and an insulator (X: oxygen or halogen) have been investigated in order to probe the character of bonds or any size-specific behavior. The study of abundance patterns in cluster mass spectra indicates the stability of clusters.[1–4] In most cases, the particular stable sizes have been well interpreted by ionic models such as the rigid ion or the polarizable ion model.[5] According to these models, the ionic clusters tend to have very well defined and regular structures. Thus the most stable structures for the mixed clusters are expected to be compact cubic ones similar to pieces of the crystal lattice. A remarkable example is the observation of a particular stability for $M_{14}X_{13}^+$ corresponding to the smallest cubic ion cluster ($3\times3\times3$). *Ab initio* calculations allow the precise determination of the geometry structure but, unfortunately, are limited to small sizes. In particular, *ab initio* calculations confirm that the small alkali halide clusters have roughly the structure of a small piece of bulk.[6,7] Another powerful tool to probe the stability of clusters is to study the decomposition pathways and the dynamics of dissociation of strongly heated clusters. For example, the results on the unimolecular decomposition of sputtered $(CsI)_nCs^+$ mixed clusters have led to the same conclusions as the study of abundance patterns in mass spectra, supporting then the ionic model.[8]

The study of hydrogenated lithium clusters is of great interest in order to explore the interaction of hydrogen atoms with a metal. Hydrogen is less electronegative than halogens. In fact, hydrogen has the peculiarity of behaving as an acceptor or a donor of an electron depending on its surrounding. LiH bulk is an ionic crystal with a NaCl structure. However, the transfer of electrons to hydrogen atoms is weaker than for NaF or NaCl crystals. Differences between alkali halide clusters and hydride of alkali clusters are expected. Former experiments and calculations showed that little Li_nH and Na_nF clusters have not the same structure.[9] While the fluorine atom strongly localizes one electron, the ionic nature of bonding in Li_nH cluster is less pronounced. In $(LiH)_n$ clusters, we do not expect a totally ionic bonding but a partial ionic bonding with a covalent part which could strongly modify the structure of these clusters compared to other ionic mixed clusters. These clusters are ideal candidates for the study of the competition between the ionic and covalent part in hydrogen bonding.

In this paper, we have studied, using a reflectron mass spectrometer, the unimolecular decomposition of $(LiH)_nLi_m^+$ ($m=0$, 1, and 3 and $n\leqslant 15$) clusters. These clusters are found to decay only by evaporating a LiH or a Li_2H_2 molecule. Simulating the evaporative rate of these clusters, which constitute an evaporate ensemble, we have also calculated, using a statistical model, the binding energies of $(LiH)_nLi^+$ and $(LiH)_nLi_3^+$ clusters. A particular model has been developed to take into account the very different vibrational frequencies in a mixed cluster. In the last section, we discuss these energies and the particular stabilities. Geometries based on compact cubic structures are suggested. The rather surprising dissociation channels of $(LiH)_nLi_3^+$ clusters are also discussed.

II. EXPERIMENT

Figure 1 displays a scheme of the experimental apparatus. Hydrogenated lithium clusters are produced in a seeded molecular beam.[10] Pure isotopic lithium ^7Li is heated in a special TZM oven up to 1200 °C, that corresponds to a vapor pressure of about 100 Torr. The lithium vapor is expanded through a 100 μm nozzle together with a few bars of argon mixed with 4% of H_2 in argon. The beam is extracted through a 1 mm skimmer and crosses the ionizing laser 20 cm after the skimmer. In this experiment, the neutral clusters are ionized with the third harmonic of a Nd:YAG laser (355 nm). With a Glan prism, we are able to monitor the laser fluence from very low fluence (1 mJ/cm^2) to very high fluence (450 mJ/cm^2) without a focusing lens and up to 1 J/cm^2 with a focusing lens. With a very high fluence laser, ionized clusters are heated which highly increases their internal energy during the 10 ns duration of the laser pulse. Rapid sequential evaporative cooling results in an ion cluster distribution shifted toward smaller masses and greatly different

 0021-9606/96/104(1)/110/10/$6.00

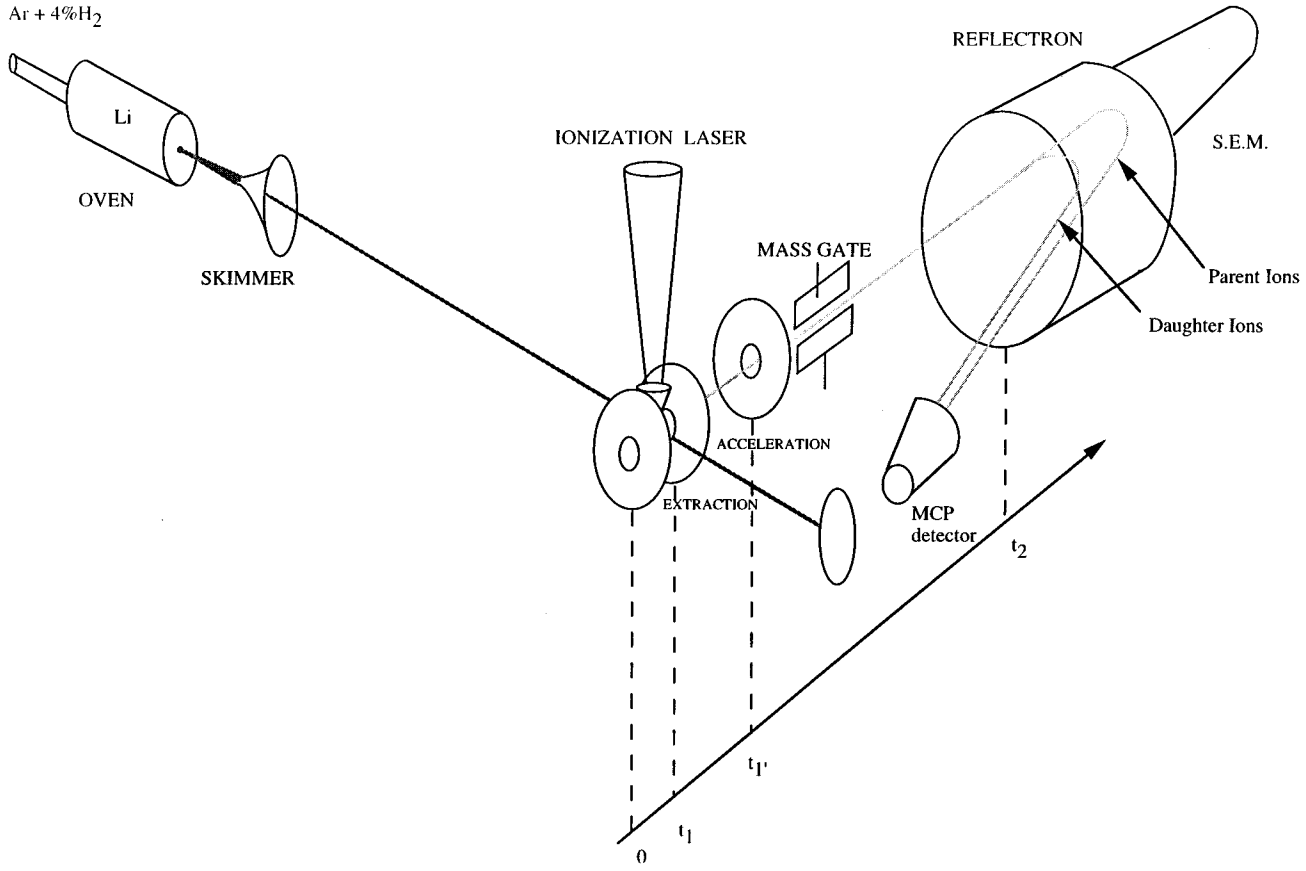

FIG. 1. Schematic diagram of the experimental apparatus. The origin of time is defined by the laser shot. t_1, t_1', and t_2 are, respectively, the residence time in the extraction region, the acceleration region and the first field free region.

from the distribution of clusters produced by the source. To determine the distribution of neutral clusters produced by the oven, we used a frequency doubled tunable dye laser to obtain the uv range which allows a direct photoionization at low laser fluence. Ionized clusters are mass selected either by a classical Wiley–MacLaren time of flight mass spectrometer or by a reflectron mass spectrometer. This second mass spectrometer allows the unimolecular evaporation of the ionized clusters to be observed.[11] Ionized clusters are extracted and accelerated by 900 V. They are then directed through a 120 cm long field-free region toward a reflectron where they are reflected. After that they travel 90 cm through a second field free region toward a detector. Parent and daughter ions born from an evaporation process in the first field region are separated in the reflectron. Indeed, if a metastable parent ion with an initial energy U_0 evaporates, the resulting daughter ion will have a kinetic energy $U_d = m_d/m_p U_0$ (where m_d and m_p are the daughter and parent masses, respectively) smaller than the parent one and then, it will have a shorter reflective travel than the corresponding parent ion. Therefore, after the second field free region, daughter ions are collected by the detector (multichannel plates) earlier than the parent ions. Note that ion clusters can be collected and mass analyzed just after the first field free region by another detector (secondary electron multiplier). A mass gate is located at the first point of the spatial focus in the first time of flight and allows one parent and its fragments to be selected. The experimental time windows (as seen in Fig. 1), for example, are about $t_1 \approx 2.0$ μs for extraction and $t_2 \approx 30$ μs for $(LiH)_{13}Li^+$. The time spent in the acceleration region t_1' is negligible compared to t_1.

III. EXPERIMENTAL RESULTS

A. Mass spectra of hydrogenated lithium ion clusters

Figure 2 shows three spectra of hydrogenated lithium clusters ionized with different photon energies and fluences. They are recorded at the end of the first field free region with a simple T.O.F. which explains a moderate resolution. Figure 2(a) displays a mass spectrum recorded with a photon energy of 4.96 eV from a dye tunable laser and at low laser fluence 1 mJ/cm^2. The energy of the photon is higher than the ionization potentials of the clusters, the laser fluence is low, the clusters are then ionized by a one-photon process. Pure lithium and hydrogenated lithium Li_nH_m are observed. Indeed, each peak is separated by 1 uma, thus between two pure lithium clusters, we observe the hydrogenated lithium clusters Li_nH, Li_nH_2 and so on. Li_nH_7 have the same mass as Li_{n+1}, and both clusters overlap in the mass spectrum. However, we observed that with the low percentage of hydrogen

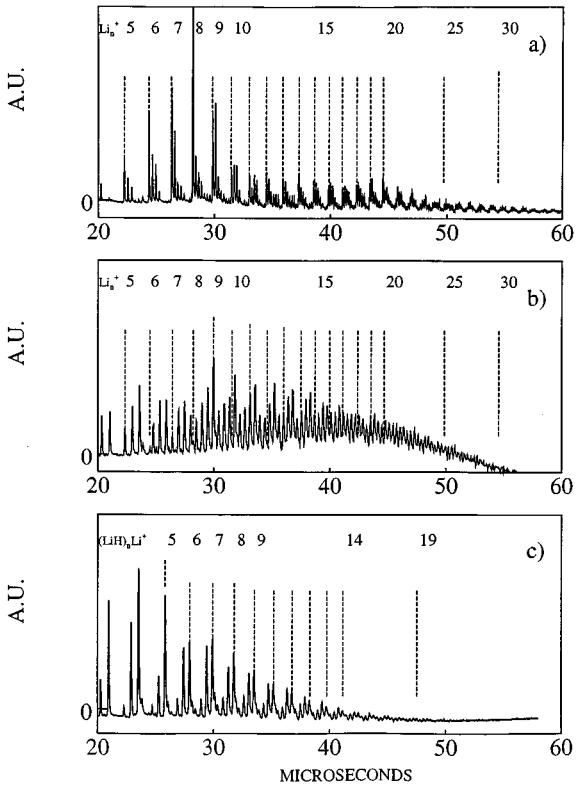

FIG. 2. Mass spectra of hydrogenated lithium cluster ions under different ionization conditions: (a) 4.96 eV energy ionization, laser fluence 1 mJ/cm^2. (b) 3.49 eV energy ionization, laser fluence 10 mJ/cm^2, (c) 300 mJ/cm^2.

used for all these experiments (4%), the intensity of Li_nH_m clusters regularly decreases with m. Figure 2(b) and 2(c) display two mass spectra recorded with the same source conditions used in Fig. 2(a) but with a lower photon energy and for two different laser fluences. This photon energy of 3.49 eV is below the ionization potentials of small clusters but from about $n=15$, one photon ionization can occur, at least for metal rich clusters.[12] For low laser fluence [Fig. 2(b)], and for large sizes, moderate resolution due to low signal avoids a simple assignment, but peaks are observed on all the channels. For small clusters, a careful analysis shows that the more intense peaks no longer correspond to pure metal clusters but to hydrogenated clusters. The peaks are mainly due to $(LiH)_nLi_m^+$ with $m=0$, 1, 3, and 5. While the spectrum 2(a) reflects the intensities of the neutral clusters in the beam, the small size clusters in spectrum 2(b) are ionized by multiphoton processes and evaporation can occur during the ionization. For high laser fluence [Fig. 2(c)], multiphoton processes are extremely significant. For example, at a laser fluence of 50 mJ/cm^2, a pure lithium cluster with around 20 atoms may absorb up to 30 photons during the laser pulse.[13] Clusters are then strongly heated implying rapid sequential evaporations and only the most stable ionic clusters are observed. The most intense series correspond to the ionized clusters $(LiH)_nLi_m^+$ with $m=0$, 1, and 3. No particular stable size with an intense peak is clearly observed but some step like features are observed, in particular after $n=13$. By comparing the two last spectra, we can see that the main distribution has been completely shifted toward the small masses due to rapid sequential evaporative cooling. As the fluence of the laser increases, only the three series $(LiH)_nLi_m^+$ ($m=0$, 1, and 3) remain. The $(LiH)_nLi_3^+$ peaks have roughly the same intensities as the $(LiH)_nLi^+$ peaks whereas the $(LiH)_n^+$ peaks are much less intense than the others. The distribution of ionized clusters is globally shifted toward smaller masses but the relative intensities of the $(LiH)_nLi_3^+$ clusters as compared to the $(LiH)_nLi^+$ clusters are constant up to fluence equal to 1 J/cm^2. The cooling by evaporation is a two step process. The source produces rich metal clusters [spectrum 2(a)]. First, the clusters evaporate monomers and dimers of lithium.[14] The clusters lose the lithium atoms in excess. This leads to the three main series which are observed on spectrum 2(c). Secondly, these clusters decay by evaporation of LiH or Li_2H_2 molecules (as we will see below). If the fluence of the laser is high, a $(LiH)_nLi^+$ cluster [respectively, $(LiH)_nLi_3^+$ cluster] which is observed in the mass spectrum comes from a $(LiH)_{n+p}Li^+$ cluster [respectively, $(LiH)_{n+p}Li_3^+$ cluster] which has evaporated several LiH molecules. This is less straightforward for $(LiH)_n^+$ clusters. The coexistence of different series is surprising and quite unusual in spectra of mixed clusters which are ionized with a high power laser.[15] The three different series evaporate LiH or Li_2H_2 molecule, so, once created, the corresponding series cannot disappear. Successive evaporations of monomers and dimers of lithium will finally lead to $(LiH)_nLi_3^+$ clusters. To explain the existence of $(LiH)_nLi^+$ series, one can notice that during the laser pulse, the internal energy of clusters reaches high values and several dissociation channels may be opened for the first evaporations. Moreover, different isomeric structures for $(LiH)_nLi_3^+$ clusters with different preferential pathways of evaporation may coexist. Some of the $(LiH)_nLi_3^+$ isomers may quickly disappear by evaporation of 2Li or Li_2 leading to the $(LiH)_nLi^+$ series. There is a competition between ionization and heating during the laser pulse. Some neutral clusters may be strongly heated and may evaporate prior to ionization. So, the observed $(LiH)_n^+$ clusters certainly reflect this process and the high stability of the neutral $(LiH)_n$ clusters.

B. Unimolecular decay of $(LiH)_nLi_m^+$ clusters

All possible unimolecular decay channels were examined for $(LiH)_nLi_m^+$ with $m=0$, 1, and 3 and $1\leqslant n\leqslant 15$ in the first field free region (t_1,t_2). Only two dissociation channels have been observed corresponding to the loss of a LiH molecule or a Li_2H_2 molecule

$$(LiH)_nLi_m^+ \rightarrow (LiH)_{n-1}Li_m^+ + LiH \quad (1)$$

$$(LiH)_nLi_m^+ \rightarrow (LiH)_{n-2}Li_m^+ + Li_2H_2 \quad (2)$$

An example of a mass spectrum resulting from unimolecular

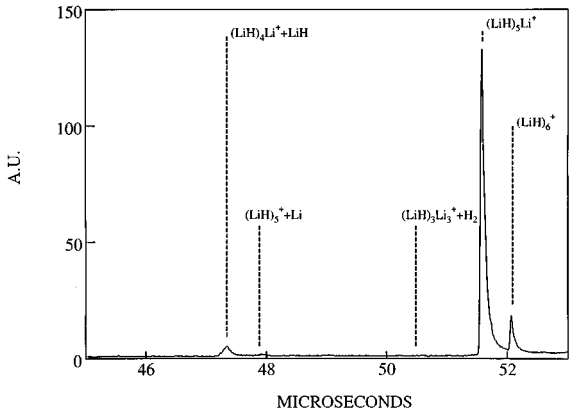

FIG. 3. Example of unimolecular dissociation during the time of flight (t_1,t_2). $(LiH)_5Li^+$ and $(LiH)_6^+$ have been selected with the mass gate.

dissociation is given in Fig. 3. The main peak on the right of the spectrum corresponds to the parents which have not evaporated and the peak on the left to fragments. On the right of the main parent peak $(LiH)_5Li^+$, we can see the $(LiH)_6^+$ cluster. Note that all the dissociation channels are very well resolved, and the assignment is not ambiguous. No H_2 or Li evaporation occurs. In the considered size domain ($n \leqslant 15$), the loss of a molecule LiH requires an energy of dissociation which is not negligible as compared to the internal energy of the evaporating cluster; therefore after an evaporation of one LiH molecule, the resulting clusters is too cold and cannot evaporate another molecule in the considered time window (10^{-5}–10^{-4} s). Whereas, the loss of a Li_2H_2 molecule requires an energy of dissociation comparable to the one corresponding to the loss of a LiH molecule. We are therefore sure that the second dissociation channel corresponds to the evaporation of Li_2H_2 and not to two successive evaporations. For larger clusters, the loss of two successive molecules LiH would occur but they have not been studied in this present paper. Surprisingly, no dissociation channel corresponding to the evaporation of a H_2 or Li_2 molecule, allowing a transfer from the $(LiH)_nLi^+$ cluster series to the $(LiH)_nLi_3^+$ cluster series and conversely, has been observed. We want to emphasize that these dissociation pathways are totally different from the pathways that we observe for metal rich clusters: Weakly hydrogenated lithium clusters $Li_nH_m^+((n-m)>3)$ dissociate along two pathways, evaporating a monomer or a dimer of lithium.[14] For each selected mass, we can define the fractional dissociation ratios

$$F_1=\frac{I_{m,n-1}}{I_{m,n}+I_{m,n-1}+I_{m,n-2}}, \tag{3}$$

$$F_2=\frac{I_{m,n-2}}{I_{m,n}+I_{m,n-1}+I_{m,n-2}} \tag{4}$$

and the total dissociation ratio

$$F=F_1+F_2=\frac{I_{m,n-1}+I_{m,n-2}}{I_{m,n}+I_{m,n-1}+I_{m,n-2}}, \tag{5}$$

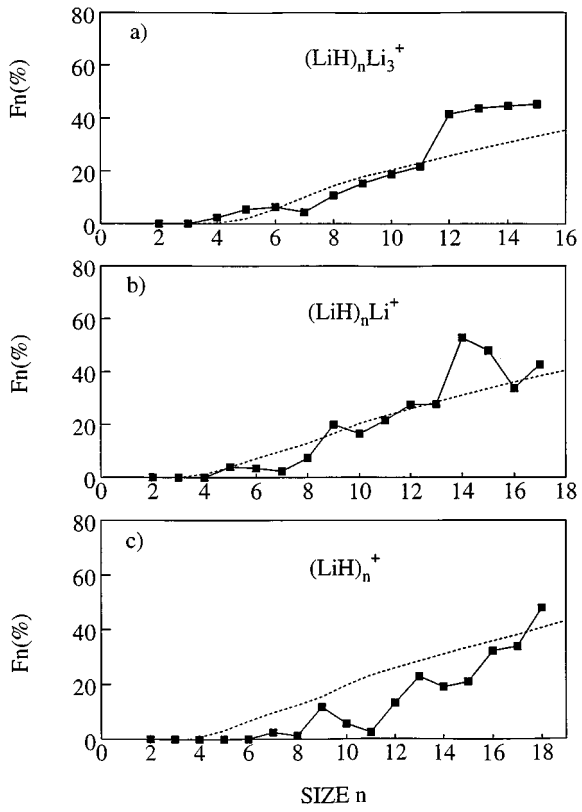

FIG. 4. Total dissociation ratio of $Li_m(LiH)_n^+$ (with $m=0$, 1, and 3) within the time (t_1,t_2) as a function of the cluster size. The full squares denote the measured total decay and the dashed line is the calculated mean trend of F as explained in the text.

where $I_{m,n}$, $I_{m,n-1}$, and $I_{m,n-2}$ are the peak intensities of the remaining parent $(LiH)_nLi_m^+$ and of their ionic fragments, respectively. In order to probe the competition between the two pathways of dissociation, we can define the branching ratio for the loss of a (LiH) molecule

$$\mathrm{Br}_1=\frac{F_1}{F}=\frac{I_{m,n-1}}{I_{m,n-1}+I_{m,n-2}}. \tag{6}$$

In Fig. 4, the total unimolecular decay rates F of $(LiH)_nLi_m^+$ (with $m=0$, 1, and 3) within the time window (t_1,t_2) are plotted. These rates present for the stoichiometric clusters, a general increase with the cluster size, with strong variation superimposed for certain masses. Some clusters have particularly a low decay rate in the mean trend; its means that these clusters have an enhancement of stability with respect to the other sizes and are relatively stable to the evaporation process. This singularity is especially observed for the $(LiH)_nLi^+$ clusters like $(LiH)_7Li^+$, $(LiH)_{10}Li^+$ and particularly for $(LiH)_{13}Li^+$. For the $(LiH)_nLi_3^+$ clusters, the same mean trend is observed but much more smooth than for the

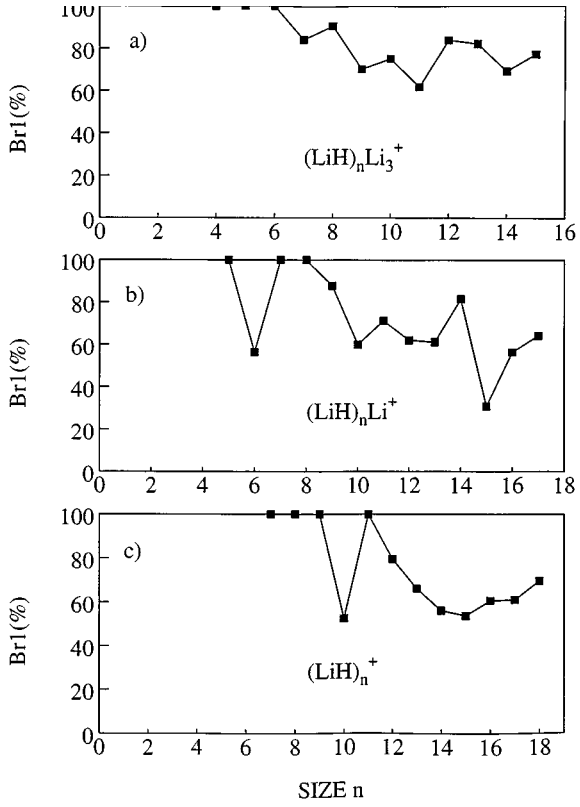

FIG. 5. Branching ratio for the loss of a LiH molecule of $(LiH)_nLi_m^+$ (with $m=0$, 1, and 3) as a function of the cluster size.

$(LiH)_nLi^+$ clusters. Lower decay rates are obtained for$(LiH)_7Li_3^+$ and $(LiH)_{11}Li_3^+$. For the $(LiH)_n^+$ clusters, the same mean trend is likewise observed with two singularities $(LiH)_8^+$, $(LiH)_{11}^+$ but the dissociation ratios are lower. Figure 5 represents the branching ratio for the loss of a LiH molecule as compared to the loss of a Li_2H_2 molecule. For small sizes, the evaporation of a LiH molecule seems to be the only decay process, the loss of Li_2H_2 molecule increases as the cluster size increases. Furthermore, we can see that for $(LiH)_nLi^+$ clusters, the size $n=15$ evaporates essentially a Li_2H_2 molecule leading to $(LiH)_{13}Li^+$ and the size $n=14$ evaporates essentially a LiH molecule leading to the same $(LiH)_{13}Li^+$. This confirms the relatively stable behavior of $(LiH)_{13}Li^+$ with respect to the evaporation process.

IV. DETERMINATION OF THE CLUSTER BINDING ENERGIES

A. Evaporative rate constant

In order to model the evaporation process of $(LiH)_nLi_m^+$ clusters, one has to determine from a simple statistical theory, an expression of the evaporative rate constant as a function of the internal energy of the cluster. If the internal energy E is assumed to be randomly distributed among the $s=3n-6$ internal vibrational modes, the rate of dissociation for a metastable cluster M_n^+ is given by the RKK classical expression[16]

$$k_n(E)=\nu g\,\frac{\omega((E-D_n),s)}{\omega(E,s)}, \tag{7}$$

where ν is the frequency of modes, g is the degeneracy pathway factor, $\omega((E-D_n),s)$ is the number of ways for arranging the energy among the s internal vibrational modes with an energy greater than D_n in a given mode; D_n is the binding energy corresponding to the dissociation channel and $\omega(E,s)$ is the number of ways of arranging an energy E among the s internal modes. If all the modes are identical

$$\omega(E,s)=\prod_{q=1}^{q=s-1}\frac{(E+qh\nu)}{qh\nu}. \tag{8}$$

This is a good approximation for a metallic cluster, but for a mixed cluster $(LiH)_nLi_m^+$, the rate of dissociation cannot be so simple. In particular, it is obvious that there are modes with very different frequencies. In the bulk, these modes would correspond to acoustic and optical phonons. The frequencies are around 32×10^{12} Hz for the optical phonons and 16×10^{12} Hz for the acoustic phonons.[17] We have considered that the internal energy E is randomly distributed among two kinds of oscillator with two different vibrational frequencies. Due to the small size of our clusters, we have taken the frequencies of the dimer ground state of Li_2 ($\nu=10.5\times10^{12}$ Hz) and LiH ($\nu=42.1\times10^{12}$ Hz) molecules.[18] They have the same order of magnitude than the optical and acoustical phonon frequencies of the bulk. The number of ways of arranging the internal energy E among the $s=s_{\mathrm{LiH}}+s_{\mathrm{LiLi}}$ internal modes is

$$\omega(E,s)=\sum_{p=0}^{p=E/h\nu_{\mathrm{LiH}}}\omega((E-ph\nu_{\mathrm{LiH}}),s_{\mathrm{LiH}})\times\omega'(ph\nu_{\mathrm{LiH}},s_{\mathrm{LiLi}}), \tag{9}$$

where $\omega((E-ph\nu_{\mathrm{LiH}}),\ s_{\mathrm{LiH}})$ and $\omega'(ph\nu_{\mathrm{LiH}},s_{\mathrm{LiLi}})$ are the numbers of ways of distributing the internal energy among the $s_{\mathrm{LiH}}=3n-6$ oscillators and $s_{\mathrm{LiLi}}=3(n+m)$ oscillators, respectively. The probability of localizing enough internal energy (equal to the fragment binding energy D_n and the average kinetic energy of the fragments ϵ[19]) in a single Li–Li mode will be given by

$$p_n(E,D_n)=\frac{\sum_{p=0}^{p=E-D_n-\epsilon/h\nu_{\mathrm{LiH}}}\omega((E-D_n-\epsilon-ph\nu_{\mathrm{LiH}}),s_{\mathrm{LiH}})\omega'(ph\nu_{\mathrm{LiH}},s_{\mathrm{LiLi}})}{\sum_{p=0}^{p=E/h\nu_{\mathrm{LiH}}}\omega((E-ph\nu_{\mathrm{LiH}}),s_{\mathrm{LiH}})\omega'(ph\nu_{\mathrm{LiH}},s_{\mathrm{LiLi}})}. \tag{10}$$

Then the rate of dissociation will be

$$k_n(E)=g\nu p_n(E,D_n). \tag{11}$$

g value is more difficult to determine. It corresponds to the degeneracy factor equal to the number of surface units capable of evaporating.[20] To determine this number, we counted the number of possible evaporative channel on little cubes or parallelepipeds with a NaCl structure. The ratio of this number on the number of atoms is roughly constant and depends very little on size and shape, the degeneracy factor is roughly equal to $3n$ for the evaporation of a LiH molecule and the half for a Li_2H_2 molecule. Lastly, the time energy distribution range is given by the highest frequency.

B. The evaporative ensemble

The model of the evaporative ensemble, widely treated by Klots,[21] leads to the knowledge of the internal energy distribution of each member of this ensemble. Ion clusters which are observed in the first field free region and born in the extraction region under a multiphoton process, form an evaporative ensemble if they dissipate their internal energy only by evaporation (which is the principal cooling process) and if they have undergone at least one evaporation. We worked under conditions for which we were sure that each cluster undergoes a large number of evaporations. We carefully checked that the fluence of the laser was sufficiently high, so that the $(LiH)_nLi^+$ and $(LiH)_nLi_3^+$ clusters have evaporated several LiH or Li_2H_2 before being extracted. Indeed, if one plots the evaporative rate of a cluster as a function of the laser fluence, the heating and then the evaporative rate of the cluster increase as the fluence increases. For high laser power, the evaporation rate reaches a limiting value. The observed ionic cluster results from a large number of sequential evaporations and then, its internal energy depends only on the characteristic time of the experiment.[21] We carefully checked so as to always work under these conditions for $(LiH)_nLi^+$ and $(LiH)_nLi_3^+$ clusters. Both cluster series form a well defined evaporative ensemble. The conditions cannot be reached for $(LiH)_n^+$. This is probably due to the competition between ionization and heating during the laser pulse. For these last clusters, the evaporations probably occur mainly before ionization. On a very rough model, one can plot the expected evaporative rate considering that all the ionic clusters of a series have the same dissociation energy D. We observe evaporation of clusters in the time window (t_1,t_2). The percentage F of the fragment ions produced during the time of flight t_2 is roughly equal to[22]

$$F\approx\frac{E(t_1)-E(t_2)}{D}, \tag{12}$$

where $E(t_1)$ and $E(t_2)$ are the internal maximal energy of the cluster parent paquet at the time t_1 and t_2, respectively (Fig. 6). $E(t_1)$ and $E(t_2)$ are given, using Eq. (10), by

$$\frac{1}{t}=\nu g p_n(E(t),D). \tag{13}$$

As the evaporation of dimer is not negligible, in this very rough model, we took into account both channels, and we used for the degeneracy factor

$$g=g_{LiH}Br_1+g_{Li_2H_2}(1-Br_1)\cong\frac{3}{2}(1+Br_1)n. \tag{14}$$

In Fig. 4, the calculated trend and experimental values of dissociation rate F for each size are plotted. The calculated curve is obtained, using Eq. (12) and (Eq. (13) where t_1 and t_2 are the two experimental times and taken a constant value of $D=2.01$ eV (the choice of this value is justified below, the curves are quite insensitive to this value). We can see that the calculated curves well reproduce the mean trends of the measured decay rates, except for $(LiH)_n^+$ where the calculated values are slightly larger than experimental results. In fact, as explained above, $(LiH)_n^+$ clusters essentially reflect a strong neutral stability and perhaps, they do not form a well defined ionic evaporative ensemble. Furthermore, the $(LiH)_n^+$ peaks are much less intense than the others, so the error on the experimental results may be significant.

C. The binding energies

A more sophisticated calculation allowed us to reproduce the singularities of the measured evaporative rates and to determine precisely the binding energies of the $(LiH)_nLi^+$ and $(LiH)_nLi_3^+$ clusters. First, the fact that two evaporative channels are observed allows to determine not only relative dissociation but absolute dissociation energies. The energy balance of the following cycle:

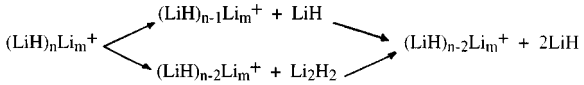

leads to

$$D_n^+(1)+D_{n-1}^+(1)-D_n^+(2)-D_{Li_2H_2}=0, \tag{15}$$

where $D_n^+(1)$ and $D_n^+(2)$ are the dissociation energies for LiH and Li_2H_2 evaporations, respectively. As no experimental values are available for the reaction $Li_2H_2\rightarrow 2LiH$, we

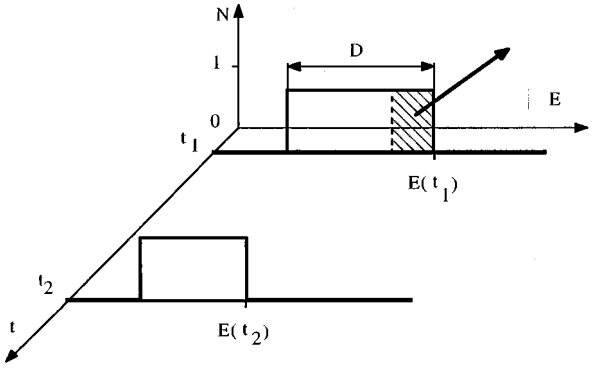

FIG. 6. Schematic of the energy distribution N of the parent population $(LiH)_nLi_m^+$ at t_1 and t_2. The dashed area represents the evaporation of high energy parents during the time of flight t_2.

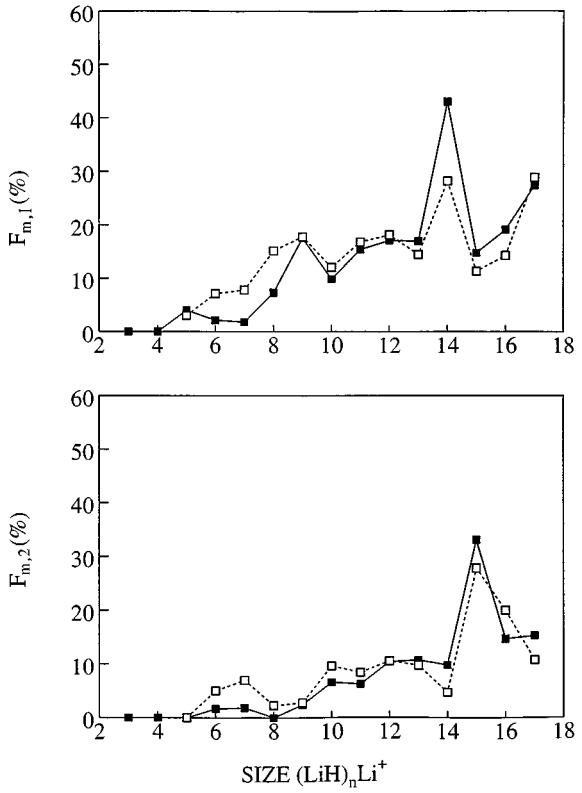

FIG. 7. Comparison of experimental and calculated values of the fractional dissociation ratios for the $(LiH)_nLi^+$ clusters. Full squares correspond to experimental rates. The open squares denote calculated values from [Eq. (17)].

used the very reliable theoretical value of Ref. 23, $D_{Li_2H_2} = 2.01$ eV. In particular, one can notice that if the two evaporation channels have equal dissociation energies, then:

$$D_{n-1}^+(1) \approx D_{Li_2H_2}. \tag{16}$$

Using this relation to roughly determine a first set of dissociation energies, we have then resolved the rate equations for the formation of $(LiH)_nLi_m^+$ cluster packet at t_1 considering that they are formed by either a LiH evaporation or a Li_2H_2 evaporation and for its evaporation during (t_2-t_1). The fractional dissociation ratio $F_{n,1}$ can be expressed as[24]

$$F_{n,1}=\frac{\int_0^\infty Q(n,E,t_1)P_{t_1t_2}(n,E,n-1)dE}{\int_0^\infty Q(n,E,t_1)dE}, \tag{17}$$

where $Q(n,E,t_1)$ is the probability that $(LiH)_nLi^+$ contains at t_1 an internal energy E and $P_{t_1,t_2}(n,E,n-1)$ is the probability for this cluster existing at t_1 to have one (LiH) evaporation before t_2. One has a similar relation for the dissociation rate $F_{n,2}$. As mentioned above, we carefully checked that no successive evaporations can occur during the time window t_1. The dissociation rate $F_{n,2}$ cannot be due to the evaporation of two monomers. Thus using $D_n^+(1), D_n^+(2)$ and the recurrence relation (15), we have adjusted their values to agree with the experimental dissociation ratios $F_{n,1}$ and $F_{n,2}$. The best fit corresponding to the evaporation of $(LiH)_nLi^+$ is plotted in Fig. 7). The agreement between experimental and theoretical values is all the more extremely good because relation (15) is always exactly verified. A similar very good fit was obtained for $(LiH)_nLi_3^+$ clusters. The corresponding dissociation energies are given in Table I and plotted in Fig. 8. They are bracketed with an uncertainly of around 0.05 eV. This error bar is weak since the two evaporation channels are often observed. However, we want to point out that these values are strongly connected to the value of the dissociation energy of Li_2H_2; a change of this value would globally shift our dissociative energies. The binding energies of $(LiH)_nLi_3^+$ exhibit a pronounced maximum for $(LiH)_{13}Li^+$ relatively to others. To a lesser extent, maxima are also obtained for $(LiH)_{16}Li^+$, $(LiH)_{10}Li^+$ and $(LiH)_7Li^+$ corresponding to a periodicity of 3 LiH units or 6 atoms. The binding energies of $(LiH)_nLi_3^+$ are more regular except for $(LiH)_{11}Li_3^+$ and $(LiH)_7Li_3^+$, and they slowly decrease with cluster size (Fig. 8) but remain very close to 2 eV.

TABLE I. Dissociation energies of $(LiH)_nLi^+$ clusters associated to the following dissociation channels: $-(LiH)_nLi^+ \rightarrow (LiH)_{n-1}Li^+ + LiH\ D_1^+$; $(LiH)_nLi^+ \rightarrow (LiH)_{n-2}Li^+ + Li_2H_2\ \ D_2^+$.

$(LiH)_nLi^+$	D_1 (eV)	D_2 (eV)
4	2.15	
5	1.99	2.13
6	1.98	1.96
7	2.07	2.04
8	2.08	2.14
9	1.98	2.05
10	2.01	1.98
11	2.00	2.00
12	1.99	1.98
13	2.08	2.06
14	1.91	1.98
15	1.94	1.84
16	2.03	1.96
17	1.96	1.98

TABLE II. Dissociation energies of $(LiH)_nLi_3^+$ clusters associated to the following dissociation channels: $-(LiH)_nLi_3^+ \rightarrow (LiH)_{n-1}Li_3^+ + LiH\ \ D_1^+$; $(LiH)_nLi_3^+ \rightarrow (LiH)_{n-2}Li_3^+ + Li_2H_2\ \ D_2^+$.

$(LiH)_nLi_3^+$	D_1 (eV)	D_2 (eV)
4	2.05	
5	2.05	2.09
6	2.02	2.06
7	2.07	2.08
8	2.03	2.09
9	2.02	2.04
10	1.99	2.00
11	2.06	2.04
12	2.01	2.06
13	1.97	1.97
14	1.99	1.95
15	1.99	1.97

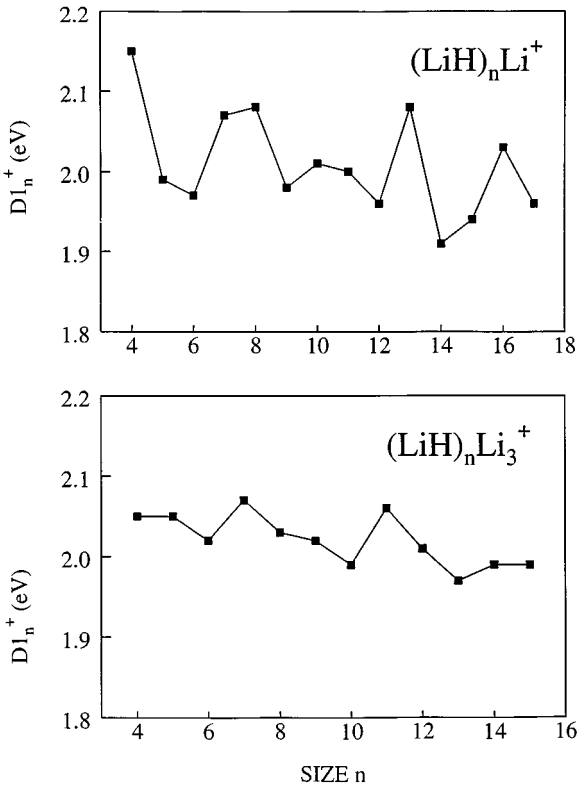

FIG. 8. Dissociation energies corresponding to the evaporation of a LiH molecule for $(LiH)_nLi^+$ and $(LiH)_nLi_3^+$ clusters.

D. Temperature of clusters

The energy distribution of a cluster may be converted to a temperature distribution by using the microcanonical definition of the temperature of a finite system

$$\frac{1}{T}=\frac{\partial S(E)}{\partial E}. \tag{18}$$

Using the binding energies, the distribution of temperature is determined for each mass entering the first field free region. For relatively large clusters, an average value of temperature can be defined. We typically found, for $(LiH)_nLi_m^+$ $(m=1,3)$ clusters, a temperature of 1000 K which is a little larger than the melting point of the bulk $T_{\mathrm{mp}}=961$ K[25] and slightly lower than the Debye temperature $T_D=1128$ K.[26] Calculations of the heat capacity of these clusters $(C_v=\partial E/\partial T)$ shows that for these temperatures, all the vibrational modes are filled.

V. DISCUSSION

Before beginning the discussion, we want to emphasize the electronic differences between alkali hydride and alkali halide salts. In a familiar picture of ionic bonding in a alkali halide MX crystal, each metal and halogen atom are respectively in the positive (M^+) and negative (X^-) forms of a closed shell ion. Hydride of lithium is an ionic crystal with the NaCl crystal structure. But, the simple assumption of a strong ionic bond for LiH crystals is rather erroneous. Indeed, the x-ray determination of the electron density distribution in the crystal gives 1.52 electrons in the Wigner–Seitz hydrogen cell as compared to 9.88 electrons in the F cell for LiF.[27] In small hydrogenated lithium clusters, the Mulliken charge in the hydrogen atom is about 1.4.[28] A covalent contribution in the LiH bond which is not taken into account in any ionic model could explain the differences between hydrides and halides. For stoichiometric hydrogenated lithium clusters, the ionic character of the bonds is expected to be closed to the character of the bulk. In a very crude approximation $(LiH)_nLi^+$ series may be represented by the familiar picture with $(n+1)Li^+$ anions and n H^- cations. In return, for the two other observed series, such a picture leads to a problem of charge excess. $(LiH)_nLi_3^+$ have two excess electrons and $(LiH)_n^+$ an excess hole. We firstly discuss the $(LiH)_nLi^+$ clusters and then the $(LiH)_nLi_3^+$ clusters.

A. $(LiH)_nLi^+$ clusters

As previously indicated, this series was the expected series. Earlier studies on various alkali halide MX clusters have found the $(MX)_nM^+$ series as the most stable series.[1–4] The dissociation energies for the evaporation of a LiH or a Li_2H_2 molecule are closed to 2 eV. This energy is twice the energy necessary to evaporate a Li atom or a Li_2 molecule in a pure lithium cluster[22] or in a metal rich lithium hydride cluster.[14] The heating of metal rich clusters leads to the evaporation of the excess metal atom, which is the most favorable evaporation pathway. The LiH dissociation energies are close to the values of the bulk. The heating of the bulk leads to the liquid phase and then to the evaporation of H_2 molecules in contradiction to the dissociation channels observed in clusters. A simple Born–Haber cycle calculation shows that in the bulk, the evaporation of a LiH requires 2.32 eV whereas those of H_2 needs 1.88 eV in the same standard conditions.[29] The two dissociation pathways are thus very close. The *ab initio* calculations of Koutecky[23] show that for very small sizes, the H_2 and LiH evaporation channels are also the most favorable. For $Li_3H_2^+$, the dissociation energy of H_2 is 1.75 eV and the dissociation energy of LiH is 1.88 eV. The calculated values are closed to the values of the bulk. However, in a finite well structured small system, the loss of two hydrogen atoms would require a total reorganization of the charge, whereas the loss of one or two LiH would not create any charge excess. Effectively, the *ab initio* calculations on very small clusters predict energy barriers for the H_2 dissociation.[30] The estimated temperature of our clusters is roughly equal to the melting temperature of the bulk and slightly lower than the Debye temperature. The absence of H_2 evaporation seems to indicate that our clusters are probably rigid. In order to interpret the observed stabilities, simple calculations in a crude ionic model are not adapted to lithium hydride clusters because they do not take into account the covalent part of the bonds. Only *ab initio* calculations seem accurate. Unfortunately, up to date results are available only for clusters smaller than those studied in this experiment. The very important stability to the evaporation process of $(LiH)_{13}Li^+$ suggests a filled simple cubic lattice structure $(3\times3\times3)$ as already observed in alkali halide clus-

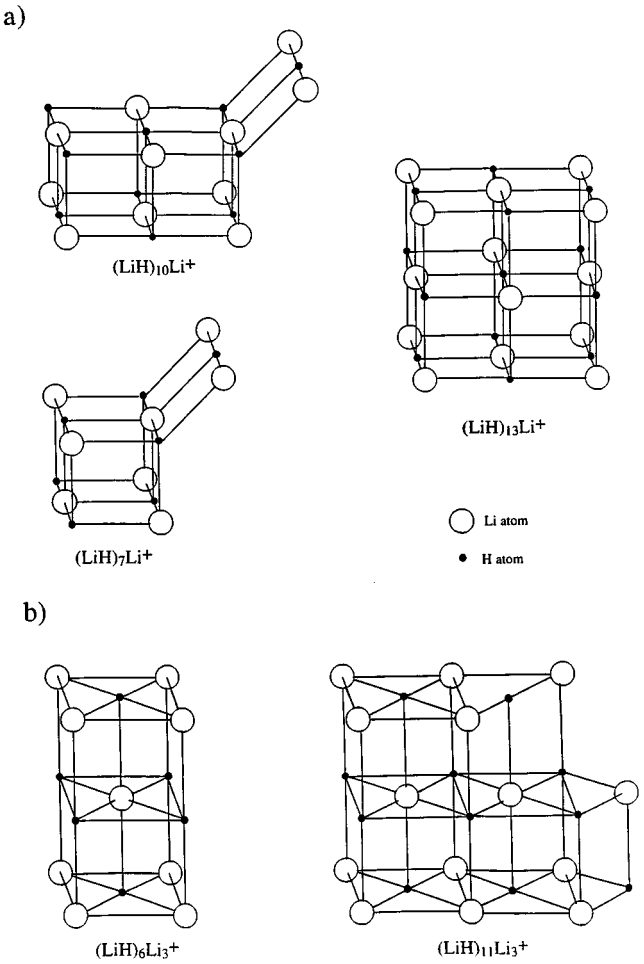

FIG. 9. Proposed structures of $(LiH)_{13}Li^+$, $(LiH)_{10}Li^+$, $(LiH)_7Li^+$ clusters (a), and $(LiH)_6Li_3^+$, $(LiH)_{11}Li_3^+$ clusters (b).

ters. The clusters may have a such simple cubic lattice structure comparable to the bulk and the evaporation would provoke a gradual peeling of the cluster. This peeling would lead to the formation of steps on a cubic structure. On the binding energies, an enhanced relative stability to evaporation decay for $(LiH)_{16}Li^+$, $(LiH)_{13}Li^+$, $(LiH)_{10}Li^+$ and $(LiH)_7Li^+$ is observed. Martin found that for $(MX)_{16}M^+$, $(MX)_{13}M^+$, $(MX)_{10}M^+$, and $(MX)_7M^+$ cubic structures are particularly stable. To stimulate theoretical calculations, we propose these structures for lithium hydride clusters. The configurations are presented on Fig. 9(a)]. We notice that these geometries correspond either to exact compact structures (3×3×3) or are very close to compact structures (4×3×3), (3×3×2), and (3×2×2) with an extra row.

B. $(LiH)_nLi_3^+$ clusters

In a crude ionic model, $(LiH)_nLi_3^+$ clusters would be constituted of $(n+3)Li^+ + nH^- 2e^-$: an ionic cluster with two excess electrons or $(n+1)\ Li^+ + nH^- + 2Li$: an ionic cluster with two excess lithium atoms. As observed for metal rich lithium hydride clusters, or other ionic clusters, we thought that these clusters would evaporate Li atoms or Li_2 molecules to lead to $(LiH)_nLi^+$ clusters. However, experimentally, these clusters evaporate LiH or Li_2H_2 molecules. This is rather surprising because energetically, the evaporation of Li or Li_2 is in principle more favorable for $(LiH)_nLi_3^+$ clusters. This is illustrated by the following thermodynamical cycle:

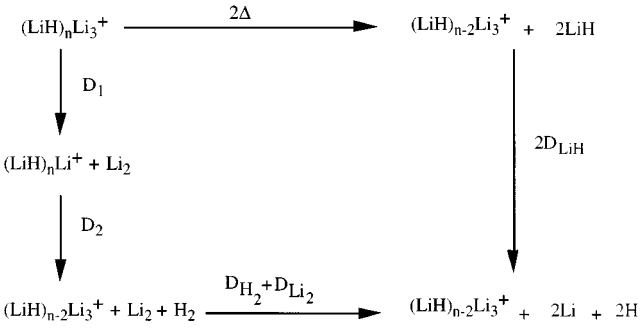

This cycle leads to

$$D_1 + D_2 = 2\Delta + 2D_{\mathrm{LiH}} - D_{\mathrm{H_2}} - D_{\mathrm{Li_2}}. \tag{19}$$

Experimental values for the dissociation of Li_2, H_2, and LiH are available. $D_{\mathrm{Li_2}} = 1.06$ eV.[31] $D_{\mathrm{H_2}} = 4.48$ eV[32] and $D_{\mathrm{LiH}} = 2.51$ eV,[33] then $D_1 + D_2 = 2\Delta - 0.52$ eV. This means that either D_1 or D_2 is less than to Δ. LiH evaporation cannot be the lowest evaporation channel for both $(LiH)_nLi^+$ and $(LiH)_nLi_3^+$ systems. To determine a numerical value for D_1, we took $\Delta = 2$ eV which is the average value we measured. As mentioned in the previous section, the H_2 evaporation energy for the $(LiH)_nLi^+$ evaporation is surely very close to the LiH dissociation energy and we took 2 eV. Then the above cycle leads to the Li_2 evaporation energy $D_1 \approx 1.4$ eV. Effectively, the *ab initio* calculations of Koutecky *et al.* show that for very small $(LiH)_nLi_3^+$ clusters like $(LiH)_2Li_3^+$, the evaporation of a Li_2 molecule is by far the lowest channel. From the energetic point of view, the Li_2 evaporation seems to be the lowest channel. However, we observe the evaporation of LiH and Li_2H_2 molecules. An energy barrier probably prevents the Li_2 evaporation. We want to emphasize that it does not appear for one or two special sizes but for the whole $(LiH)_nLi_3^+$ series that we observed ($n \geqslant 4$). This anomaly is not fully explained but a few remarks can be made. First, the clusters are observed with a high power laser. They come from metal rich clusters which have evaporated lithium atoms or molecules. There may be other stable structures that we were not able to observe. Such isomeric forms have been recently observed in $(CsI)_n^-$ clusters, depending on the source conditions.[34] In particular if these clusters were directly produced in the neutral beam, the structures might be different. Second, the organization of the structures is such that the evaporation of Li_2 is unlikely. This suggests that Li_2 is not segregated in surface of $(LiH)_nLi^+$ clusters but is fully integrated in the structure of the cluster. If the lithium excess increases, a segregation between a metallic part and an insulating part occurs. No more than two excess lithium atoms can be integrated in the insulating part. Finally, referring to the rough ionic model used for MX alkali halide clusters, the most pertinent question is how the charge corresponding to the two excess electrons is distributed. Recently, Xia and

Bloomfield[35] have studied this problem in negatively charged $(NaCl)_nNa^-$ clusters. The excess electrons tend to be localized on anion vacancies or on a Na^+ cation (to form a Na^- anion). The localization of two ''excess'' electrons in $(LiH)_nLi_3^+$ clusters is a very different problem because their role is also to avoid the Coulomb explosion of a hypothetical $(LiH)_nLi_3^{+++}$ cluster. It would be interesting to compare the dissociation channels of $(MX)_nM_3^+$ clusters and of $(LiH)_nLi_3^+$ clusters (M alkali atom and X halogen). Unfortunately, the dissociation pathways of $(MX)_nM_3^+$ clusters have not been extensively studied, even if the series $(MX)_nM_3^+$ is not usually observed in mass spectra. Nevertheless, we think that the partially covalent character of the bond in LiH renders easier the accommodation of excess electrons in $(LiH)_nLi_3^+$ clusters. It will be very fruitful for the comprehension of mixed metal–hydrogen systems to know how the charge excess is exactly distributed, it may be diluted inside the cluster, concentrated on a surface (it would constitute a metallic plan on the surface of the cluster) or may be localized on a Li^- cation. A structure built around a Li_3^+ has also been suggested but contrary to H_3^+, Li_3^+ is not particularly compact and stable.

To conclude, we propose several geometries for these clusters. They are based only on geometrical considerations. Very compact structures can be built for these clusters by addition of LiH molecules on a $(LiH)_6Li_3^+$ core. The six hydrogen atoms constitute an octahedron with a central lithium atom. Two examples are displayed on Fig. 9(b). These clusters have the structure of the bulk. All the atoms are fully integrated into the structure and the evaporation of a LiH molecule seems to be the simple way to evaporate without having to reorganize the structure.

VI. CONCLUSION

Mass spectra of highly hydrogenated lithium cluster ions are obtained by multiphoton ionization with a high power laser, of a metal rich cluster beam. Three series of clusters are observed $(LiH)_nLi_3^+$, $(LiH)_nLi^+$ and $(LiH)_n^+$. These clusters are studied by measuring their unimolecular evaporative rates in an evaporative ensemble. The three series of clusters have the same dissociation channels: the evaporation of a LiH or Li_2H_2 molecule. Contrary to the LiH bulk, no evaporation of H_2 is observed even in the stoichiometric situation $[(LiH)_nLi^+$ or $(LiH)_n^+]$. This is probably the indication for the existence of a barrier for this process, under our experimental conditions. A simple statistical model is introduced for the calculation of the evaporative rates, allowing us to measure the binding energy values corresponding to the two observed dissociation channels. The high stability of $(LiH)_{13}Li^+$ suggests for $(LiH)_nLi^+$ clusters a compact cubic structure similar to pieces of LiH crystal. The absence of Li or Li_2 evaporation for $(LiH)_nLi_3^+$ appears also particularly interesting. The stability and the dissociation pathways that we observed are not yet fully understood. But our results indicate that probably an energy barrier prevents the dissociation toward the Li_2 channel. Finally, in order to stimulate *ab initio* calculations, we have also proposed for $(LiH)_nLi_3^+$ clusters, a cubic structure built around an octahedron.

ACKNOWLEDGMENTS

The authors would like to thank M. Boudeulle and P. Mélinon for very fruitful discussions during the course of this work and V. Bonacic-Koutecky for providing us the results of their calculations prior to publication and for helpful comments.

[1] W. Ens, R. Beavis, and K. G. Standing, Phys. Rev. Lett. **50**, 27 (1983).
[2] R. Plfaum, P. Pfau, K. Sattler, and E. Racknagel, Surf. Sci. **156**, 165 (1985).
[3] E. C. Honea, M. L. Homer, P. Labastie, and R. B. Whetten, Phys. Rev. Lett. **63**, 394 (1989).
[4] P. J. Ziemann and A. W. Castleman, Jr., J. Chem. Phys. **94**, 718 (1991).
[5] J. Diefenbach and T. P. Martin, J. Chem. Phys. **83**, 4585 (1985).
[6] V. Bonacic-Koutecky, C. Fuchs, J. Gaus, J. Pittner, and J. Koutecky, Z. Phys. D **26**, 192 (1993).
[7] C. Ochsenfeld and R. Ahlrichs, J. Chem. Phys. **101**, 5977 (1994).
[8] H. J. Hwang, D. K. Sensharma, and M. A. El-Sayed, J. Phys. Chem. **93**, 5012 (1989).
[9] B. Vezin, Ph. Dugourd, C. Bordas, D. Rayane, M. Broyer, V. Bonacic-Koutecky, J. Pittner, C. Fuchs, J. Gaus, and J. Koutecky, J. Chem. Phys. **102**, 2727 (1995).
[10] J. Blanc, V. Bonacic-Koutecky, M. Broyer, J. Chevaleyre, Ph. Dugourd, J. Koutecky, C. Scheuch, J. P. Wolf, and L. Woste, J. Chem. Phys. **96**, 1793 (1992).
[11] B. A. Mamyrin, V. I. Karataev, D. V. Shmikk, and V. A. Zagulin, Sov. Phys.-JETP **37**, 45 (1973).
[12] B. Vezin, Ph. Dugourd, D. Rayane, P. Labastie, J. Chevaleyre, and M. Broyer, Chem. Phys. Lett. **206**, 521 (1993).
[13] C. Brechignac, Ph. Cahuzac, J. Leygnier, and A. Sarfati, Phys. Rev. Lett. **70**, 2036 (1993).
[14] R. Antoine, Ph. Dugourd, D. Rayane, and M. Broyer (to be published).
[15] C. W. S. Conover, Y. A. Yang, and L. A. Bloomfield, Phys. Rev. B **38**, 3517 (1988).
[16] L. S. Kassel, J. Phys. Chem. **32**, 225 (1928); **32**, 1065 (1928).
[17] M. P. Verma and R. K. Singh, J. Phys. C **4**, 2749 (1971).
[18] K. P. Huber and G. Hertzberg, *Spectra of Diatomic Molecules*, Vol. II (Van Nostrand, New York, 1959).
[19] P. C. Engelking, J. Chem. Phys. **85**, 3103 (1986); **87**, 936 (1987).
[20] W. Forst, *Theory of Unimolecular Reactions* (Academic, New York, 1973).
[21] C. E. Klots, J. Chem. Phys. **83**, 5854 (1985); Z. Phys. D **5**, 83 (1987); J. Phys. Chem. **92**, 5864 (1988).
[22] C. Brechignac, Ph. Cahuzac, F. Carlier, M. de Frutos, J. Leygnier, and J. Ph. Roux, J. Chem. Phys. **99**, 6848 (1993).
[23] V. Bonacic-Koutecky (private communication).
[24] C. Brechignac, H. Busch, Ph. Cahuzac, and J. Leygnier, J. Chem. Phys. **101**, 6992 (1994).
[25] *CRC Handbook of Chemistry and Physics*, 72nd ed. (CRC, Cleveland, 1991/92).
[26] B. W. James and H. Kheyrandish, J. Phys. C **15**, 6321 (1982).
[27] R. Brill, *Solid State Physics*, edited by F. Seitz and D. Turnbull (Academic, New York, 1967), Vol. 20, pp. 1–35.
[28] B. K. Rao, S. N. Khanna, and P. Jena, Phys. Rev. B **43**, 1416 (1991).
[29] R. C. Bowmann, Jr., J. Phys. Chem. **75**, 1251 (1971).
[30] K. Przybylski, J. Koutecky, V. Bonacic-Koutecky, P. Von Ragué-Schleyer, and M. F. Guest, J. Chem. Phys. **94**, 5533 (1991).
[31] J. Vergès, R. Bacis, B. Barakat, P. Carrot, S. Churassy, and P. Crozet, Chem. Phys. Lett. **98**, 203 (1983).
[32] A. Balakrishnan, V. Smith, and B. P. Stoicheff, Phys. Rev. Lett. **68**, 2149 (1992).
[33] K. R. Way and W. C. Stwalley, J. Chem. Phys. **59**, 5298 (1973).
[34] H. W. Sarkas, L. H. Kidder, and K. H. Bowen, J. Chem. Phys. **102**, 57 (1995).
[35] P. Xia and L. A. Bloomfield, Phys. Rev. Lett. **70**, 1779 (1993).